Interval velocity estimation from beam-stacked data — 2-D estimation results

Biondo Biondi

ABSTRACT

Perturbations caused by a velocity anomaly in the offsets and traveltimes of beam-stacks computed from finite-difference data are well predicted by ray tracing. Therefore ray tracing can be effectively used in an estimation algorithm that reconstructs the velocity model from beam-stacked data. The estimation method that I presented in previous reports (Biondi, 1988a; Biondi, 1988b) has successfully estimated a velocity anomaly from reflections off a dipping bed. The estimated anomaly is well focused, given the limitations in angular coverage of the anomaly, because beam-stacked data provide detailed information on the velocity model.

The preliminary analysis of a field dataset shows that the effects of a velocity anomaly on beam stacks can be easily measured from real data.

INTRODUCTION

In previous reports I presented a method for estimating interval velocity in geologically complex areas (Biondi, 1988a; Biondi, 1988b). The method tomographically fits a velocity model to pre-stack data, which is transformed by a beam stack (Kostov and Biondi, 1987) along the offset direction and by a local slant stack (Hermont, 1979) along the midpoint direction. Unlike most tomographic methods (Harlan and Burridge, 1983; Bishop et al., 1985; Sword, 1987), the proposed algorithm does not require data picking. Instead, it maximizes beam-stack energy at traveltimes and surface locations predicted by the velocity model. In this respect my estimation method resembles the approaches of Toldi (1985) and Fowler (1988), which maximize stacking energy as a function of stacking velocity and migration velocity.

While stacking and migration velocities depend on reflection moveouts averaged on the whole cable, beam stacks depend on the local behavior of the reflections.

Consequently the inversion of beam stacks has the potential of achieving more resolution than the inversion of stacking or migration velocities. On the other hand the measures of beam-stack parameters are less robust than the measures of stacking velocities, or migration velocities, because fewer traces are used in computing beam stacks, and thus the signal to noise ratio is lower.

In SEP-57 (Biondi, 1988a) I successfully tested the method in the particular case of a horizontally-layered medium. In SEP-59 (Biondi, 1988b) I presented the theory for evaluating the gradient of beam-stack energy with respect to a general 2-D velocity model. In this paper I test the method effectiveness in estimating a 2-D velocity anomaly from beam stacks of a synthetic dataset that was modeled by a finite-difference program.

In the next section I review the proposed estimation method. In the section on the synthetic data I examine the effects of a velocity anomaly on the offsets and traveltimes of beam-stack energy's peaks. Perturbations measured from beam-stacked data are compared with the perturbations that ray tracing had predicted. In the section on the estimation results I show the results of estimating velocity from beam stacks modeled using ray tracing and the results from the beam stacks of the finite-difference data. In the last section I show some examples of beam stacks computed from real data containing a velocity anomaly.

INTERVAL-VELOCITY ESTIMATION METHOD

In this section I review the velocity estimation method that I use to estimate velocity from beam-stacked data. The method is the same as the one I presented in previous reports (Biondi, 1988a; Biondi, 1988b) except for equation (1b) that is generalized to handle reflectors of any dip.

The estimation starts from the pre-stack data transformed by use of a beam stack along the offset direction and a local slant stack along the midpoint direction. The amplitudes of the transformed data are computed evaluating a coherency function, such as semblance, along the stacking trajectory.

The transformed data, $Beam(y, h, t, p_y, p_h)$, are functions of five variables: midpoint y, half-offset h, midpoint ray parameter p_y, offset ray parameter p_h, and traveltime t. The amplitude of beam-stacked data is proportional to the energy of the reflected waves recorded with observed horizontal ray parameters p_y and p_h, at midpoint y, half-offset h, and traveltime t.

Estimating the interval velocity in the original beam-stack domain can be problematic (Biondi, 1987). Therefore I introduce the following transformations of coordinates:

$$\tau = t - p_h h, \tag{1a}$$

$$\xi = h - \frac{p_{heq}(p_h, \hat{p}_y, \hat{V})\hat{V}^2}{4} t, \tag{1b}$$

where $\hat{V}$ is a constant average velocity and $\hat{p}_y$ is a convenient midpoint ray parameter, as for example the predominant time dip in the data. The purpose of the transformation (1b) is to concentrate the beam-stacked data around $\xi = 0$ so that storage space is saved; the expression of p_{heq} as a function of p_h, $\hat{p}_y$ and $\hat{V}$ is derived in Appendix A.

Defining an objective function

The velocity estimation is a tomographic fitting to beam-stacked data of traveltimes and surface locations predicted by the velocity model. The transformed offset ξ, as a function of transformed traveltime τ and midpoint y, is computed by use of ray tracing for each reflector point R_j and for all ray parameters p_h and p_y. The function $\xi = \xi(y(R,\mathbf{m}), \tau(R,\mathbf{m}), p_y, p_h, \mathbf{m})$ defines a manifold in the data space. The goal of inversion is to maximize the energy in beam-stacked data on the manifold $\xi = \xi(y, \tau, p_y, p_h, \mathbf{m})$. The inversion is formulated as the solution of the non-quadratic optimization problem of finding the maximum with respect to the slowness model of the total energy

$$E(\mathbf{m}) = \sum_{p_y} \sum_{p_h} \sum_{j} \overline{Beam}(y_j, \xi(y_j, \tau_j, p_y, p_h, \mathbf{m}), \tau_j, p_y, p_h), \tag{2}$$

or in more compact notation

$$E(\mathbf{m}) = \sum_{i} B_i(\xi_i(\mathbf{m})), \tag{3}$$

where i is the index of the data points used, including all reflector locations R_j and all ray parameters p_y and p_h.

Computing the gradient of the objective function

The maximum of $E(\mathbf{m})$ can be found with a gradient algorithm. Implementation of a gradient algorithm requires that the gradient of the objective function be computed with respect to the model. The gradient can be expressed as

$$\nabla E_{\mathbf{m}} = \sum_{i} \frac{\partial B_i(\xi_i(\mathbf{m}))}{\partial \mathbf{m}} = \sum_{i} \frac{\partial \xi_i}{\partial \mathbf{m}} \frac{\partial B_i(\xi_i)}{\partial \xi_i} = \mathbf{G}^T \mathbf{D}_1, \tag{4}$$

where the derivatives are computed at fixed values of y, τ, p_y and p_h.

The vector $\mathbf{D}_1$ is easily computed from beam-stacked data with a finite-difference approximation of the derivative operator. This vector represents the interaction of the inversion algorithm with the actual data.

To evaluate the Frechet derivatives the following relation is used:

$$\left.\frac{\partial \xi}{\partial \mathbf{m}}\right|_{(\bar{y},\bar{\tau},\bar{p}_y,\bar{p}_h)} = \left.\frac{\delta \xi}{\delta \mathbf{m}}\right|_{(\bar{R},\bar{p}_y,\bar{p}_h)} - \left.\frac{\delta y}{\delta \mathbf{m}}\right|_{(\bar{R},\bar{p}_y,\bar{p}_h)} \left.\frac{\partial \xi}{\partial y}\right|_{(\bar{\tau},\bar{p}_y,\bar{p}_h,\mathbf{m})} - \left.\frac{\delta \tau}{\delta \mathbf{m}}\right|_{(\bar{R},\bar{p}_y,\bar{p}_h)} \left.\frac{\partial \xi}{\partial \tau}\right|_{(\bar{y},\bar{p}_y,\bar{p}_h,\mathbf{m})}. \tag{5}$$

Partial derivatives $\partial\xi/\partial y$ and $\partial\xi/\partial\tau$ are evaluated by the use of finite differences on the manifold defined by $\xi = \xi(y, \tau, p_y, p_h, \mathbf{m})$, at constant ray parameters $\bar{p}_y$ and $\bar{p}_h$, velocity model $\bar{\mathbf{m}}$, and constant transformed traveltime $\bar{\tau}$ or midpoint $\bar{y}$, but at varying reflector point R. Total derivatives with respect to the velocity model $\delta\xi/\delta\mathbf{m}$, $\delta y/\delta\mathbf{m}$ and $\delta\tau/\delta\mathbf{m}$, are computed by use of the ray-tracing method presented in SEP–57 (Biondi, 1988b), for fixed reflector point $\bar{R}$, and ray parameters $\bar{p}_y$ and $\bar{p}_h$, but at varying transformed traveltime τ, transformed offset ξ, and midpoint y.

SYNTHETIC DATASET

To test the velocity estimation method in this paper I use a synthetic dataset generated by a finite-difference program for propagating acoustic waves. I modeled an off-end seismic survey with the geophones on the right side of the shots and for the velocity model shown in Figure 1. The background velocity is equal to 2.5 km/s and the circular velocity anomaly is a Gaussian function with peak velocity of 2.8 km/s. The velocity anomaly is estimated with the reflections from a bed dipping at 20°.

I sorted the data in 175 common midpoint gathers (CMP), spaced 20 m. The minimum offset is 20 m and the maximum offset is 1500 m with offset sampling of 40 m. Figure 2 shows the nearest offset section of the dataset. The time pull-out in the middle of the section is caused by the velocity anomaly.

The effects of the velocity anomaly on beam-stacked data

The velocity anomaly perturbs reflections from the dipping bed and consequently the beam-stacked data. I will first examine the effects of the anomaly on beam-stacks because the perturbations in traveltimes and offsets of the beam-stacks are the information that I use in reconstructing the velocity anomaly. Then, because the estimation method models by ray tracing the behavior of beam stacks, I will compare the perturbations caused by the velocity anomaly on the finite-difference data with the perturbations that were predicted by ray tracing.

Figure 3 shows the gather recorded at the midpoint location of 1700 m and the beam-stack decomposition of the gather corresponding to two different offset ray parameters, $p_{h,1}$ equal to .0535 s/km and $p_{h,2}$ equal to .0705 s/km. The curves superimposed on the beam-stacked data show the offsets as a function of traveltimes, modeled by ray tracing, when the velocity is constant and equal to the true background velocity. The offset curves pass through the beam-stacks' peaks because the reflections recorded at this specific midpoint location are not affected by the anomaly.

Figure 4 shows the gather recorded at the midpoint location of 2950 m and the corresponding beam-stack panels. The reflections recorded at this midpoint location have been perturbed by the anomaly and therefore the offset curves computed under

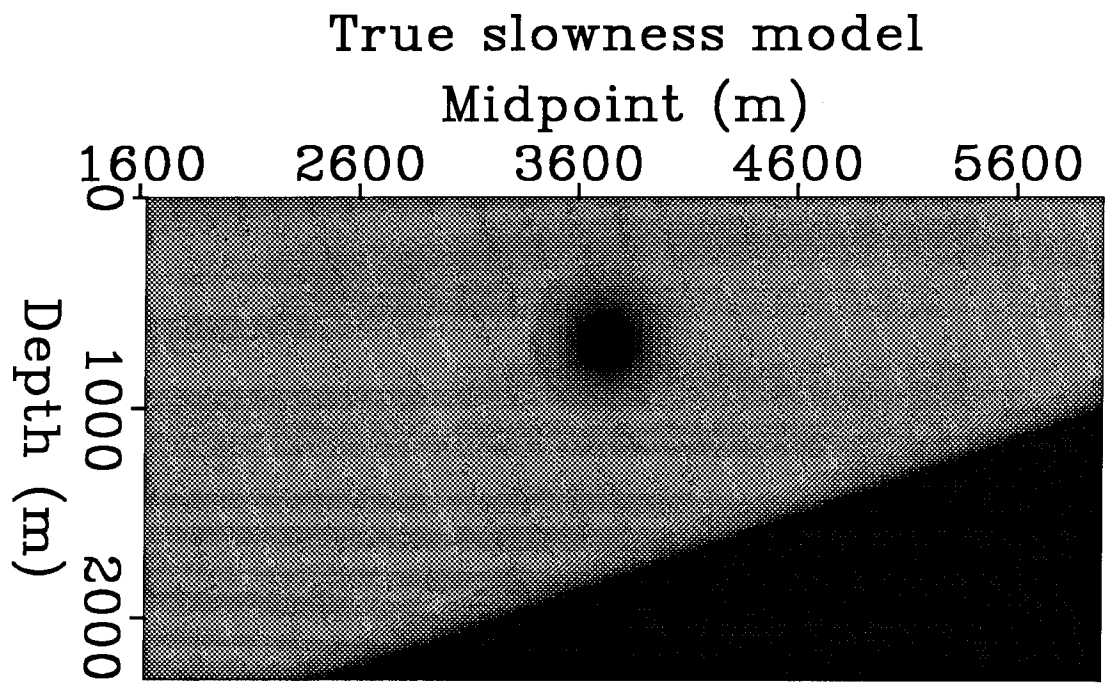

FIG. 1. The velocity model used to model the synthetic data. The background velocity is 2.5 km/s and the circular velocity anomaly is a Gaussian function with peak velocity of 2.8 km/s. The dipping reflector has a dip angle of 20°.

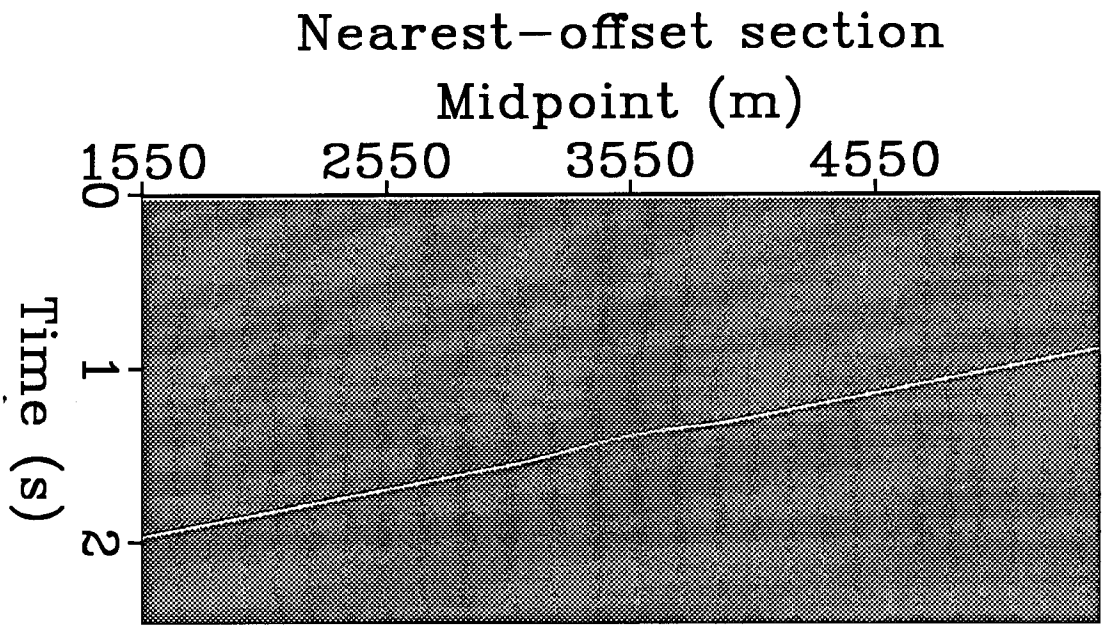

FIG. 2. The nearest-offset section of the synthetic dataset. The time pull-out in the middle of the section is caused by the velocity anomaly.

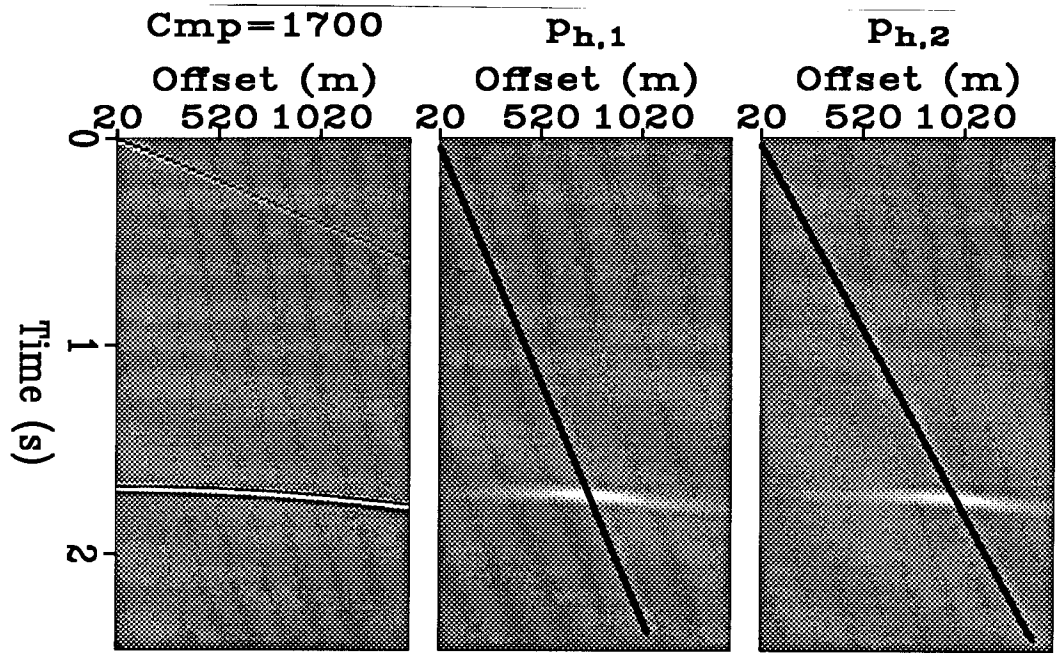

FIG. 3. The CMP gather recorded at the midpoint location of 1700 m and the beam-stack decomposition of the gather corresponding to two different offset ray parameters. The curves superimposed on the beam-stacked data show the offset as a function of traveltimes computed under the assumption of a constant velocity of 2.5 km/s. The offset curves pass through the beam-stacks' peaks because the reflections recorded at this midpoint location have not been perturbed by the velocity anomaly.

the assumption of a constant velocity model do not pass through the beam-stacks' peaks. Figure 5 shows a graphic explanation of the reason why the perturbed offsets are smaller than the unperturbed ones for this particular CMP gather. The unperturbed ray-paths (solid lines) and the perturbed ray-paths (dashed lines) are constrained to have the same offset ray parameters and the same midpoint. The raypath of the up-going ray passes above the anomaly and deviates away from it because the velocity perturbation is positive. The combination of the ray-path perturbation and of the geometric constraints causes the offset of the perturbed reflection to be larger than the offset of the unperturbed reflection. The anomaly also causes a perturbation in the midpoint ray parameter of the reflections; that is, the time dips in the midpoint direction. This effect is related to the time pull-up caused by the anomaly.

Figure 6 shows another gather close to the anomaly, recorded at the midpoint location of 3450 m, and the corresponding beam-stack panels. For this midpoint location the perturbed offset of beam-stacks is smaller than the unperturbed one because the up-going ray-path passes below the anomaly instead of above it (Figure 7). The raypath of the up-going ray still deviates away from the positive velocity anomaly but in this case the perturbation causes a decrease in the offset instead of an increase.

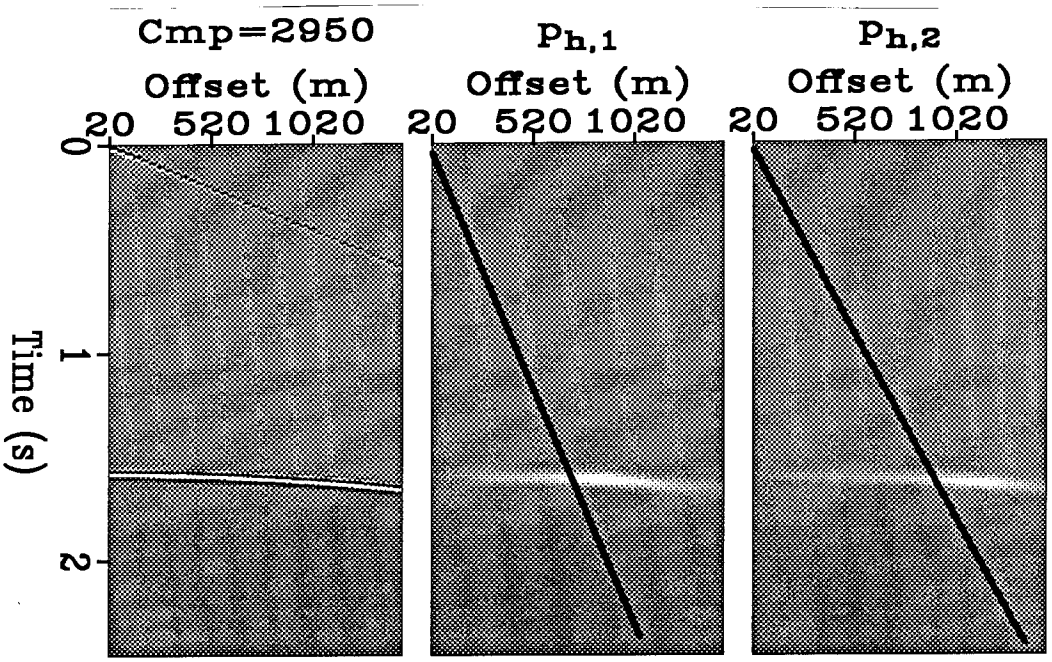

FIG. 4. The CMP gather recorded at the midpoint location of 2950 m and the beam-stack decomposition of the gather corresponding to two different offset ray parameters. The curves superimposed on the beam-stacked data show the offset as a function of traveltimes computed under the assumption of a constant velocity of 2.5 km/s. The offset curves do not pass through the beam-stacks' peaks because the reflections recorded at this midpoint location have been perturbed by the velocity anomaly.

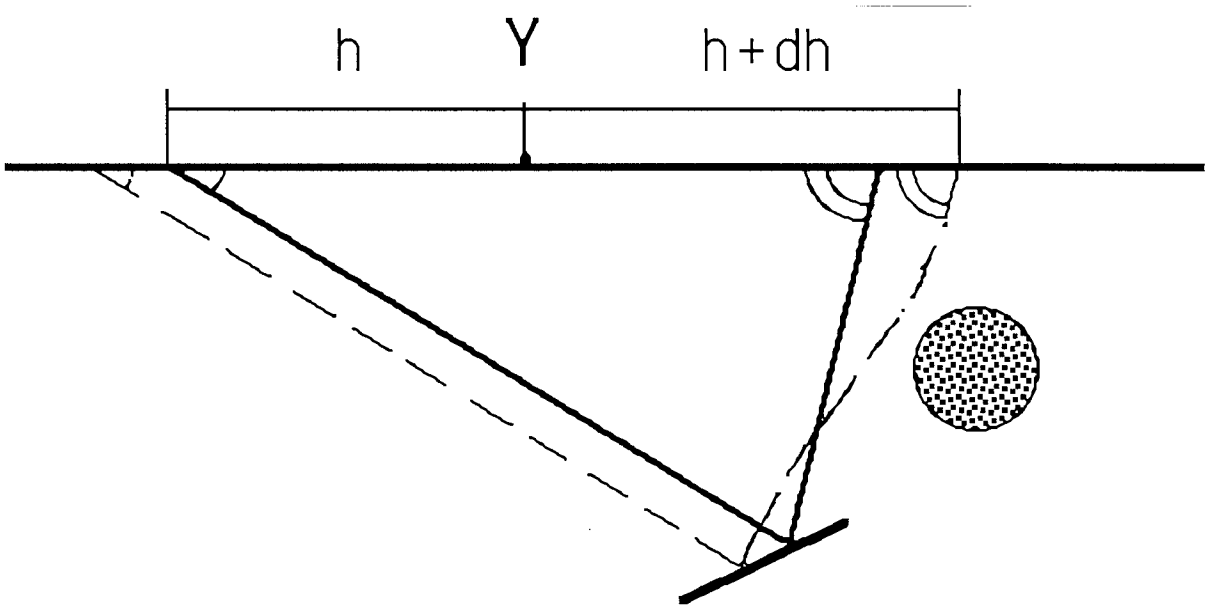

FIG. 5. The offset of the perturbed reflection (dashed line) is larger than the offset of the unperturbed reflection (solid line) because the up-going ray passes above the anomaly and deviates away from it.

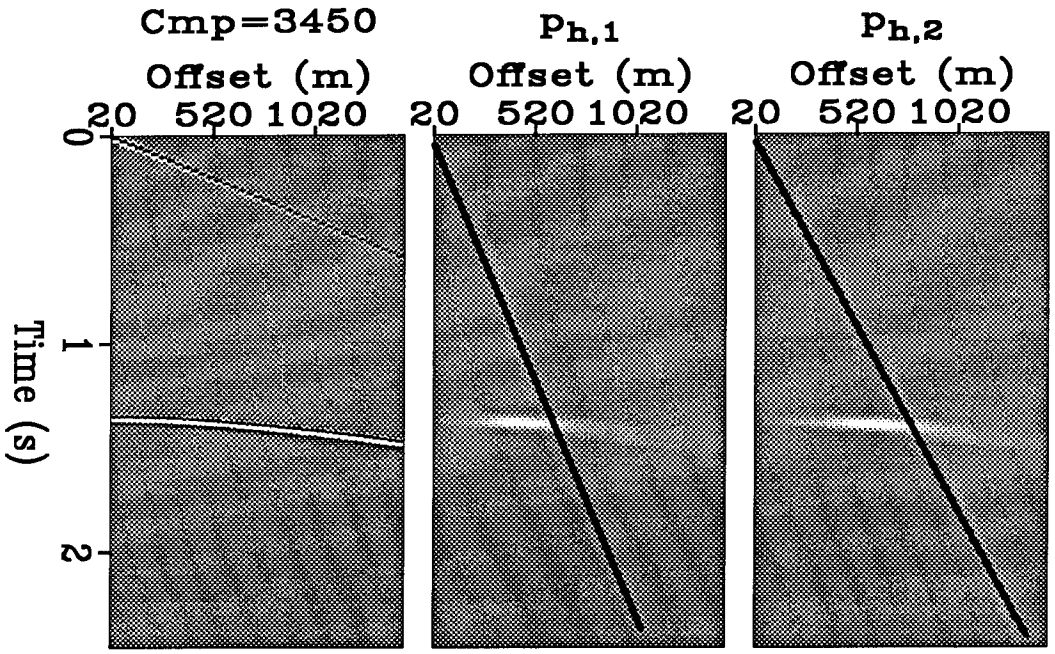

FIG. 6. The CMP gather recorded at the midpoint location of 3450 m and the beam-stack decomposition of the gather corresponding to two different offset ray parameters. The curves superimposed on the beam-stacked data show the offset as a function of traveltimes computed under the assumption of a constant velocity of 2.5 km/s. The offset curves do not pass through the beam-stacks' peaks because the reflections recorded at this midpoint location have been perturbed by the velocity anomaly.

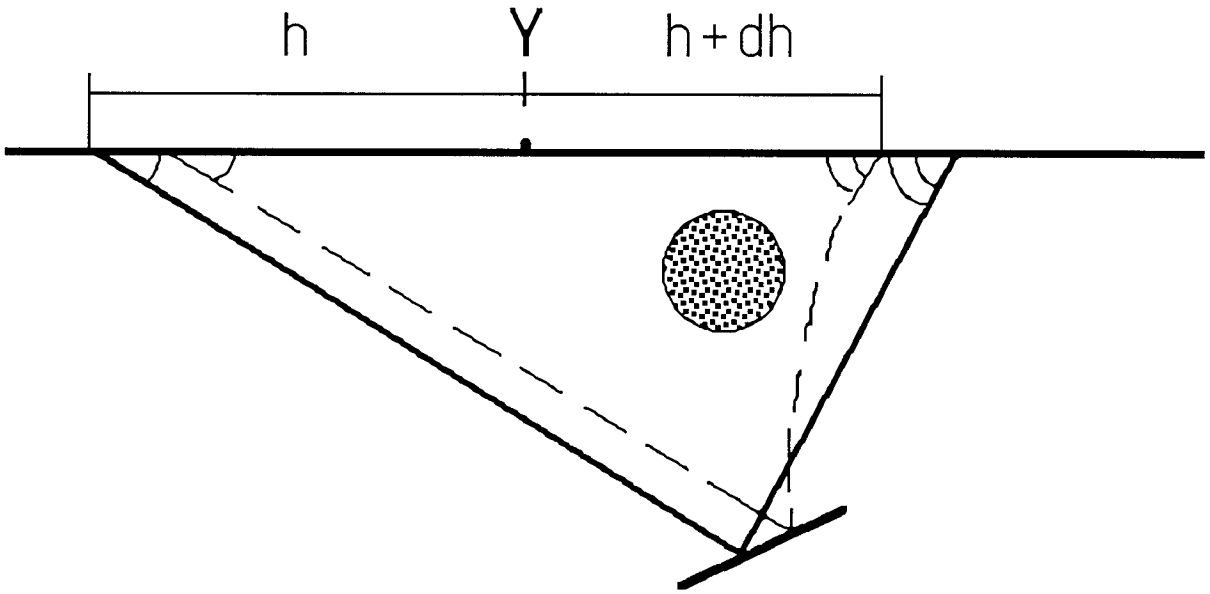

FIG. 7. The offset of the perturbed reflection (dashed line) is smaller than the offset of the unperturbed reflection (solid line) because the up-going ray passes below the anomaly and deviates away from it.

Figure 8 shows the offset of beam-stacks peaks as a function of midpoint location for all the midpoints in the dataset. The lower line shows the offset corresponding to the offset ray parameter $p_{h,1}$, while the upper line shows the offset corresponding to the offset ray parameter $p_{h,2}$. The positive perturbations in offset around the midpoint 2900 are caused by the up-going rays passing above the anomaly. The negative perturbations around the midpoint 3550 are caused by both the up-going rays and the down-going rays passing below the anomaly, while the second positive lobe is caused by the down-going rays passing above the anomaly. The traveltimes of beam-stacks' peaks as a function of midpoint location are shown in Figure 9. The traveltime perturbations have a pattern similar to the offset perturbations but their amplitudes are much smaller relative to the total traveltime.

The velocity estimation method uses ray tracing to model the behavior of beam-stacked data. Therefore, for the estimation procedure to succeed, the ray tracing must correctly predict the offsets and traveltimes of the beam-stacks' peaks. Figure 10 shows the comparison of the offsets predicted by ray tracing (solid line) and the offsets picked from the beam-stacked data (dotted line) for the offset ray parameter $p_{h,1}$. Figure 11 shows the same comparison for the traveltimes of beam-stacks. These two figures demonstrate that the behavior of beam-stacks can be well predicted with ray tracing.

ESTIMATION RESULTS

The previous section examined the effects of a velocity anomaly on beam-stacked data and showed that these effects can be well predicted with ray tracing. This section presents the results of estimating the anomaly. First I show the estimation results from the data modeled with ray tracing; then I show the estimation results from the beam stacks of the data modeled using finite difference.

Estimation results from ray-traced data

The velocity model can be estimated with a classic least-squares inversion technique that minimizes the differences between the transformed offsets computed by ray tracing through the velocity anomaly and the ones predicted by ray tracing through the estimated velocity model. The results obtained in this ideal case show the advantages and limitations of estimating velocity from beam stacks. In the inversion I used a Gauss-Newton optimization algorithm (Gill et al., 1981) and I evaluated the gradient of beam-stacks with respect to the velocity model by use of the linear operator presented in SEP-59 (Biondi, 1988b).

Figure 12 shows the transformed offsets computed by ray tracing through the velocity anomaly for six different offset ray parameters p_h: from p_h equal to .04 s/km to p_h equal to .095 s/km. The data have been transformed according to the transformations in equations (1) and assuming $\hat{V}$ equal to 2.5 km/s and $\hat{p}_y$ equal

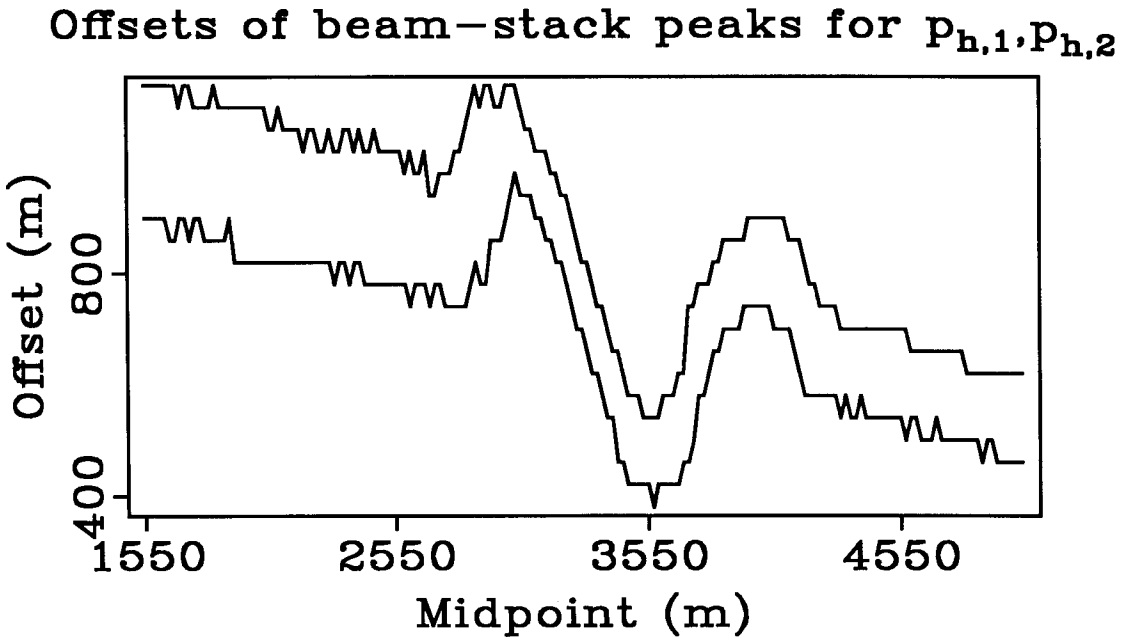

FIG. 8. The offsets of the beam-stack peaks as a function of midpoint location for two different offset ray parameters.

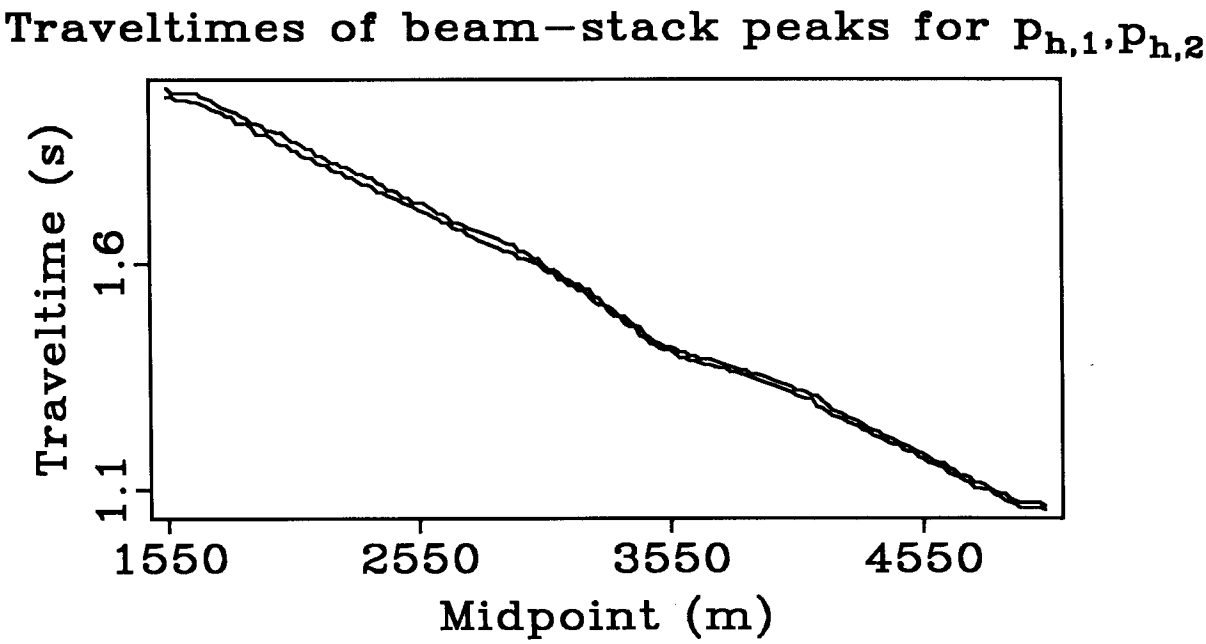

FIG. 9. The traveltimes of the beam-stack peaks as a function of midpoint location for two different offset ray parameters.

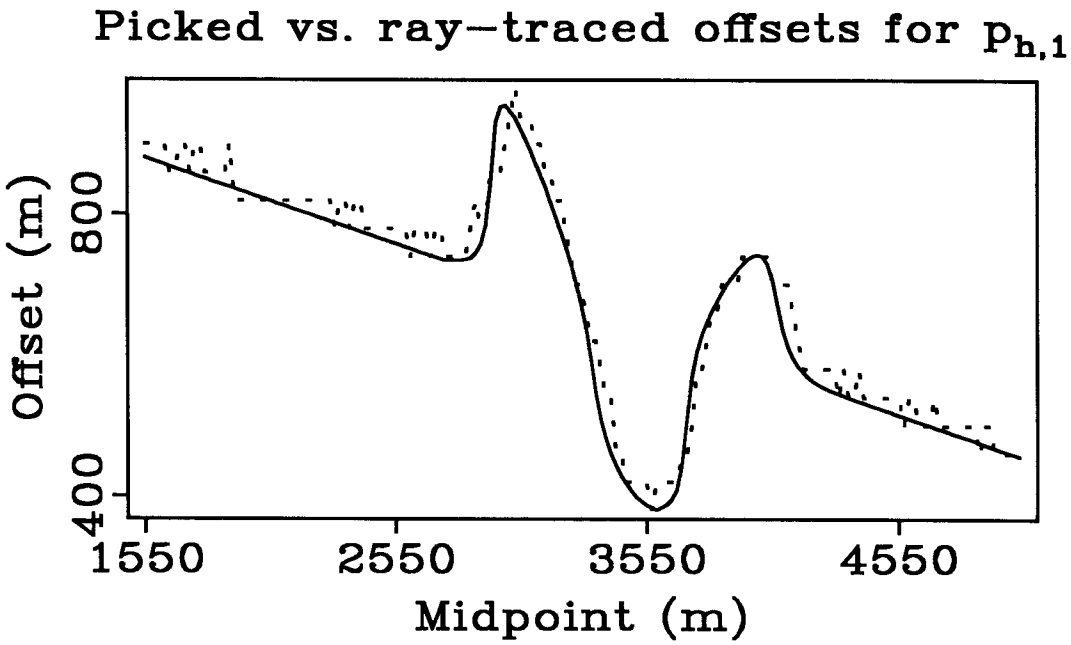

FIG. 10. The comparison of the offset predicted by ray tracing (solid line) and the offsets picked from beam-stacked data (dotted line).

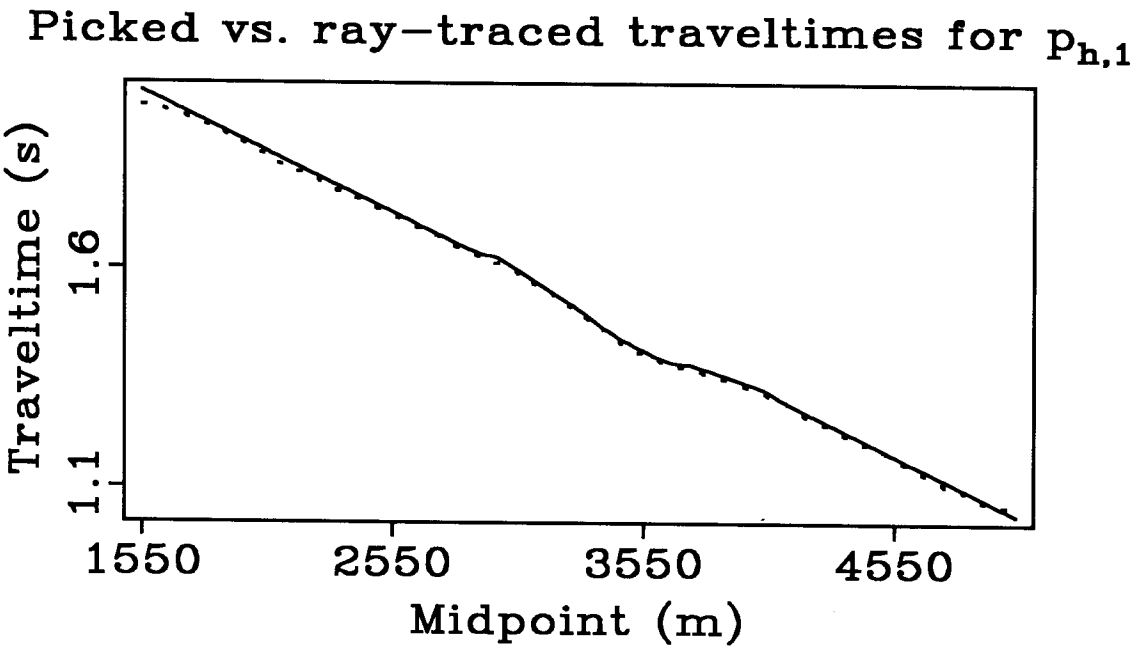

FIG. 11. The comparison of the traveltimes predicted by ray tracing (solid line) and the offsets picked from beam-stacked data (dotted line).

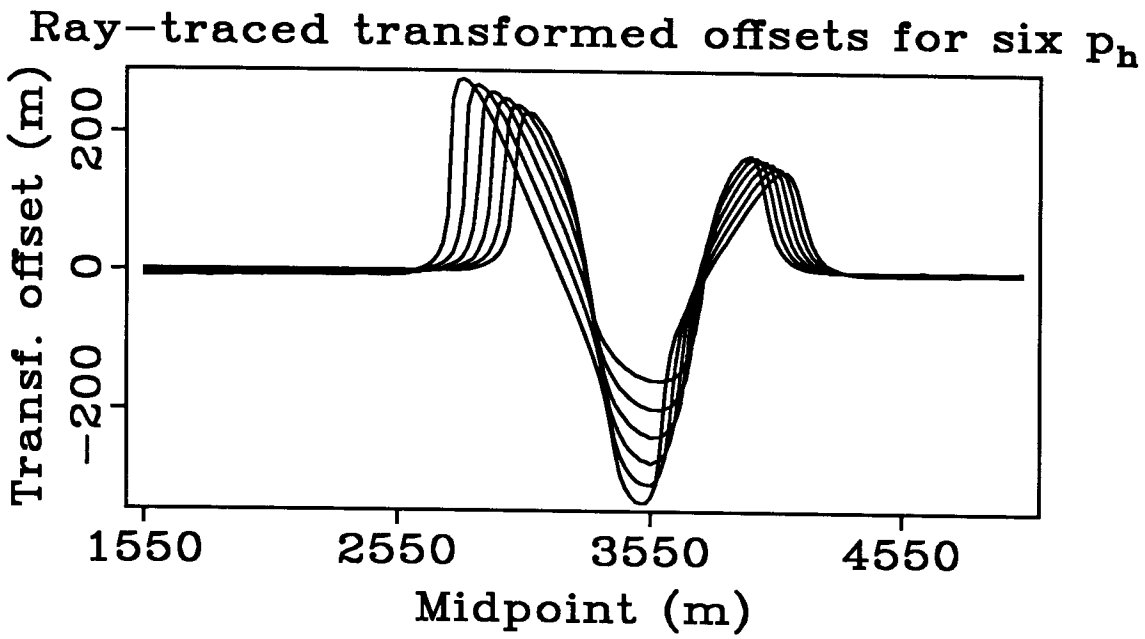

FIG. 12. The transformed offsets computed ray tracing through the velocity anomaly for six different offset ray parameters. The anomaly causes different perturbations of the transformed offset for different ray parameters because the corresponding rays pass through the anomaly at different angles.

to -.273 s/km; that is the background velocity and the midpoint ray parameter of the unperturbed reflections.

The anomaly causes different perturbations of the transformed offset for different ray parameters; the narrowest perturbation pattern corresponds to the lowest p_h, while the widest pattern corresponds to the highest p_h. The rays corresponding to the lower ray parameters pass through the anomaly more vertically than the rays corresponding to the higher ray parameters. Therefore the angular coverage of the anomaly is proportional to the range of p_h available, which depends on the maximum offset of the data. The use of multiple ray parameters decreases the null space of the relation between velocity and the data and consequently increases the resolution of the inversion.

The estimation algorithm minimized the error in transformed offsets (Figure 12) at the transformed time and midpoint ray parameters modeled by ray tracing. Figure 13 shows the result of the first iteration of the Gauss-Newton algorithm. Figure 14 shows a horizontal cross section of the slowness model shown in Figure 13 (dashed line) compared with the true model (solid line). The cross sections were taken at the depth of the center of the true velocity anomaly; that is at a depth of 700 m. The peak of the estimated anomaly is at a depth of 570 m. The optimization algorithm can be iterated if the problem is linearized around the estimated solution.

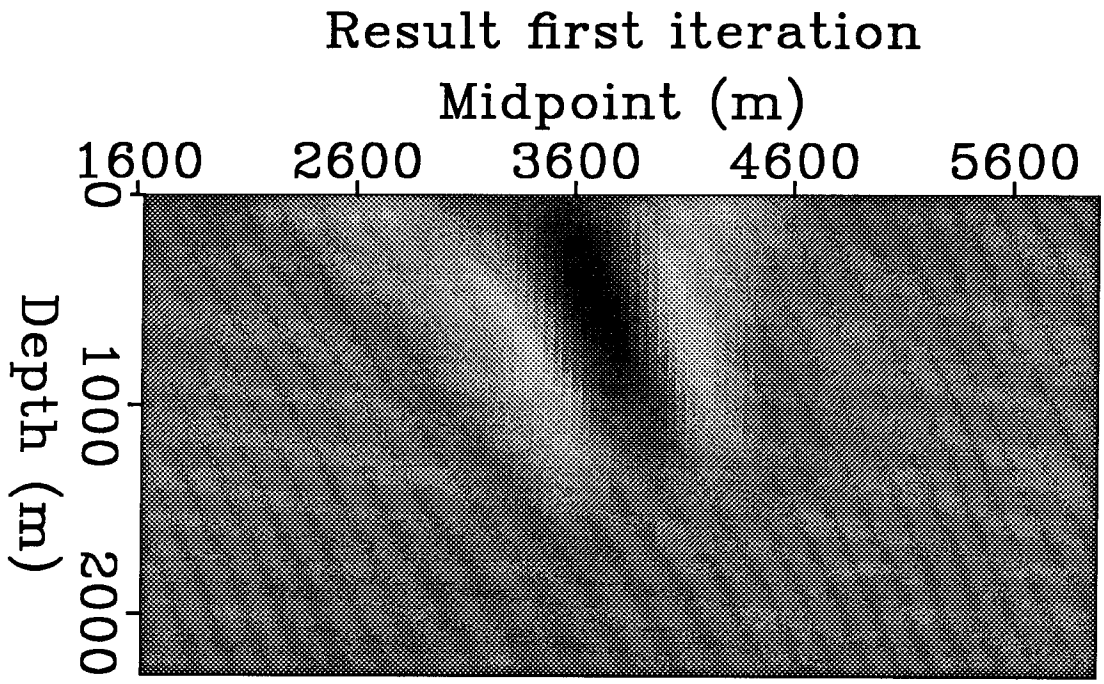

FIG. 13. The result of the first iteration of the velocity estimation from the data modeled using ray tracing. The limited angular coverage of the anomaly causes the smear of the estimated anomaly along the direction perpendicular to the reflector, and the positive side-lobes at its sides.

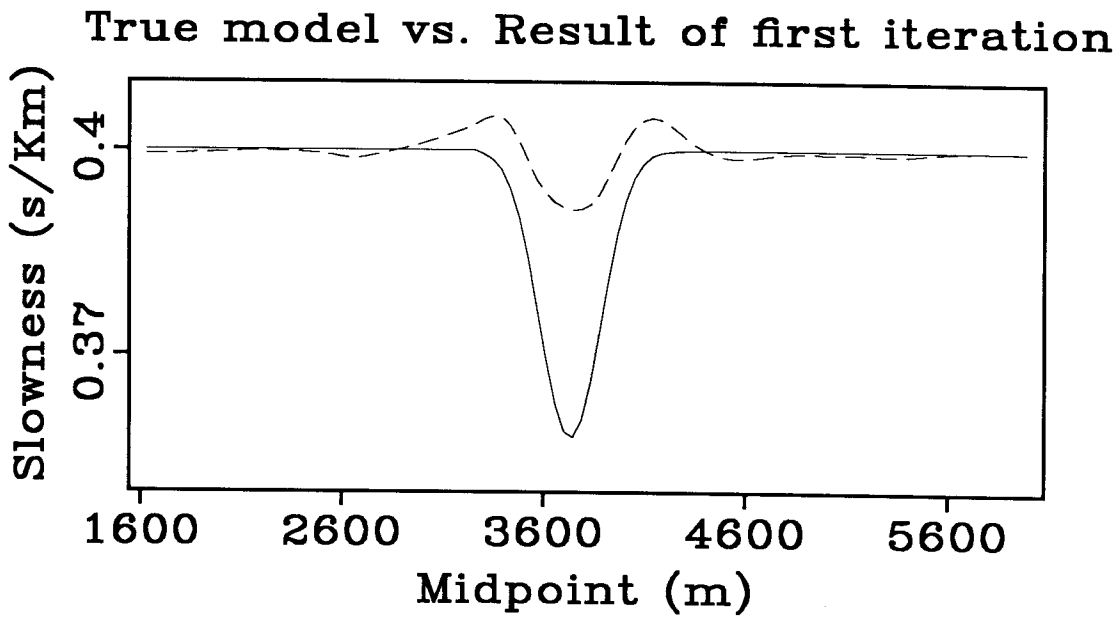

FIG. 14. A cross section of the slowness model shown in Figure 13 (dashed line) compared with the true model (solid line). The cross sections were taken at the depth of the center of the velocity anomaly; that is at a depth of 700 m.

Figure 15 and Figure 16 show the estimated velocity after seven nonlinear iterations. The anomaly estimated after the seventh iteration (Figure 15) is better focused than the anomaly estimated after the first iteration (Figure 13); therefore the amplitude of the anomaly (Figure 16) is also closer to the true amplitude than before.

The result is the expected one from a tomographic estimation of a velocity anomaly using the reflections from a single reflector (Stork, 1988; Fowler, 1988). The smear of the estimated anomaly along the direction perpendicular to the reflector and the positive side-lobes at its sides are caused by the components of the velocity model contained in the null space of the relation between the model and the data. The null space is reduced because I used multiple ray parameters but is not empty because of the limited ray coverage of the anomaly. The ray coverage depends on the cable length (1500 m) and on the reflectors' geometry and thus it would improve if there were more than one reflector.

The result of the last iteration is significantly better than the result of the first iteration. The improvements in the result achieved by the nonlinear iterations can be explained by two combined effects: first, the linearization improves when the estimated model is closer to the true model; and second, the null space of the linearization is slightly different at each iteration, and thus some velocity model components underdetermined in the first iteration can be better determined in the following ones.

Estimation results from beam-stacked data

Estimating velocity from data modeled by ray tracing is equivalent to use picked data, in the ideal case that no errors have been made in picking the data. When the data are contaminated by noise picking becomes difficult, and the picking errors might not follow the Gaussian distribution, on which the least-squares inversion is based. Therefore the proposed velocity estimation method does not use picked data but maximizes semblance of the beam-stacked data for increasing the reliability of the results.

I estimated the velocity anomaly directly from the beam-stacked data after having decomposed the data for six different offset ray parameters p_h: from p_h equal to .04 s/km to p_h equal to .095 s/km, and for seven midpoint ray parameters from p_y equal to -.333 s/km to p_y equal to -.213 s/km. I transformed the beam-stacked data according to the coordinate transformations introduced in equations (1) assuming $\hat{V}$ equal to 2.5 km/s and $\hat{p}_y$ equal to -.273 s/km. I also used a Gaussian window to smooth the transformed data along the time and midpoint axis. The optimization problem of maximizing semblance in the beam-stacked data is highly non-quadratic; therefore for improving the convergence of the algorithm I used few conjugate gradient iterations followed by Gauss-Newton iterations (Biondi, 1988a).

Figure 17 shows the result of the last, and fifth, iteration of the estimation algorithm. Figure 18 shows a horizontal cross section of the slowness model shown

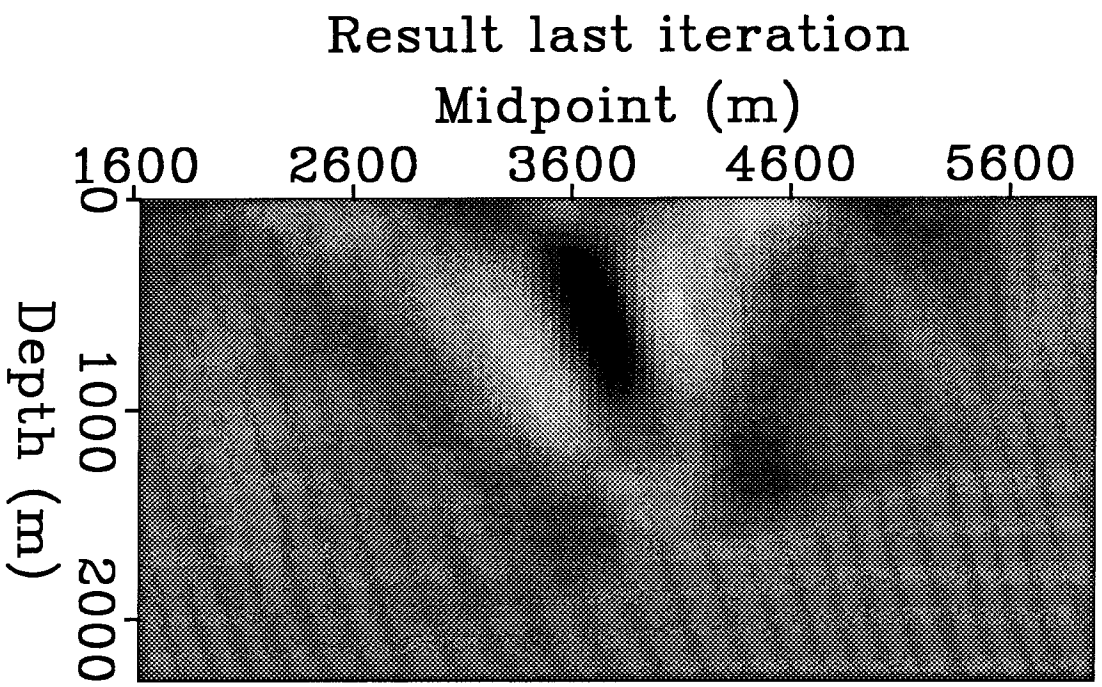

FIG. 15. The result of the seventh and last iteration of the velocity estimation. The estimated anomaly is better focused than the anomaly estimated by the first

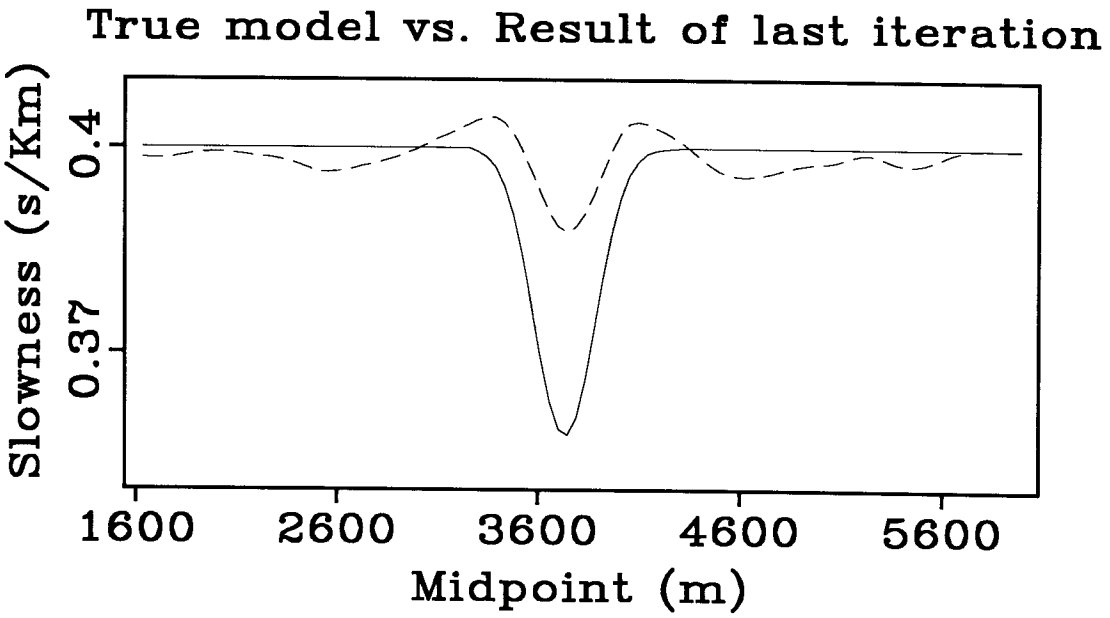

FIG. 16. A cross section of the slowness model shown in Figure 15 (dashed line) compared with the true model (solid line). The cross sections were taken at the depth of the center of the velocity anomaly; that is at a depth of 700 m. The amplitude of the estimated anomaly is closer to the true amplitude than is the result of the first iteration (Figure 14).

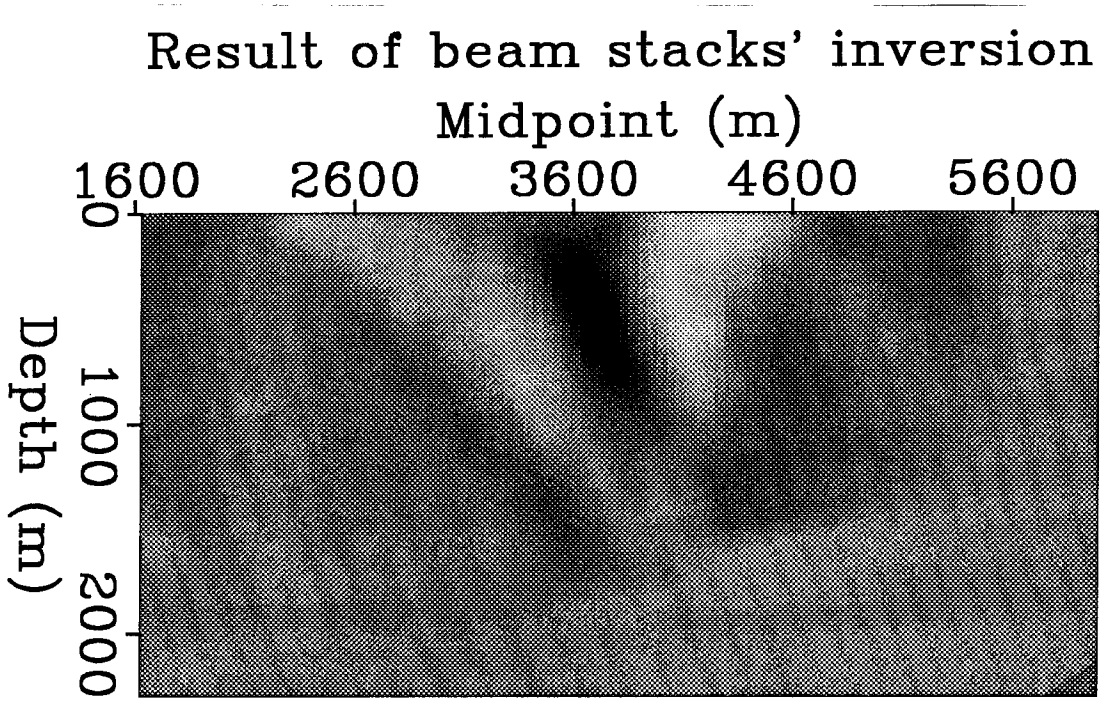

FIG. 17. The result of the last iteration of the velocity estimation from the beam-stacked data. The estimated anomaly is fairly well localized, although it is less focused than the anomaly estimated with an inversion of the ray-traced data.

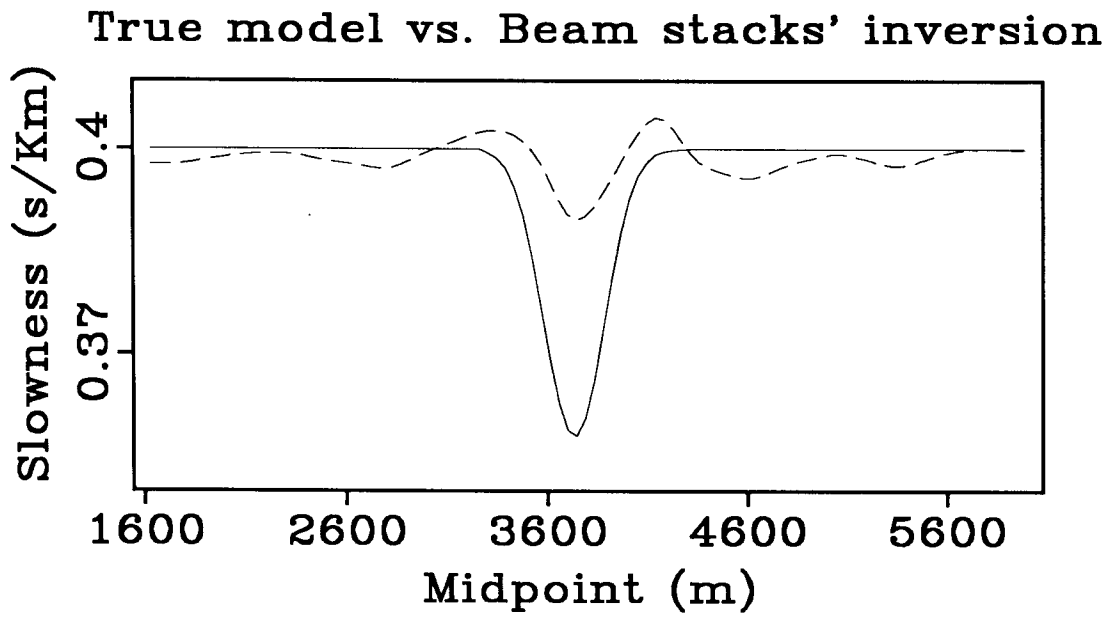

FIG. 18. A cross section of the slowness model shown in Figure 17 (dashed line) compared with the true model (solid line). The cross sections were taken at the depth of the center of the velocity anomaly; that is at a depth of 700 m.

in Figure 17 (dashed line) compared with the true model (solid line). The cross sections were taken at the depth of the center of the velocity anomaly; that is, at a depth of 700 m. The estimated anomaly is fairly well localized, although is less focused than the anomaly estimated by an inversion of the ray-traced data. There is a trade-off between the resolution of inverting picked data and the robustness of maximizing semblance.

REAL DATASET

I will be testing my velocity estimation method on a marine dataset donated to SEP by Agip. Figure 19 shows the nearest-offset section of the data. The data is particularly interesting for testing a velocity estimation method because of a low-velocity anomaly that causes the time pull-downs on the nearest-offset section near the midpoint location of 7 km. Furthermore, the velocity anomaly is on the top of an anticline and thus the effects of structure must be taken in account for estimating velocity correctly.

I have not yet tried to estimate the anomaly, but I computed the beam-stack decomposition of the data and checked to see if the velocity anomaly caused the expected perturbations in the transformed offsets of beam stacks. Figure 20 shows the transformed beam stacks for two values of the offset ray parameter p_h at the midpoint location of 6.650 km, which is just above the anomaly. Figure 21 shows the beam stacks for the same values of p_h, but at midpoint location of 7.650 km, which is at the right of the anomaly. The black lines superimposed on the beam-stacked data show the transformed offset as a function of the transformed traveltimes predicted by the laterally invariant background velocity profile shown in Figure 22. As expected, at the midpoint location above the anomaly the transformed offsets are larger than the ones predicted by the background velocity (Figure 20), while at the midpoint location further to the right (Figure 21) the transformed offsets of the reflections are lower than the one predicted by the background velocity.

For flat reflectors the behavior of beam-stacked data as a function of midpoint location is better shown by constant transformed-time slices. In this case the reflectors are not flat but the velocity anomaly has almost flattened in time the reflections coming from the top of the anticline. Figure 22 shows semblance, as a function of the transformed offset and midpoint location, at the transformed time correspondent to the reflection at around 1.8 seconds on the nearest-offset section and for p_h equal to .11 s/km. The perturbation pattern caused by the anomaly is similar to the perturbation patterns predicted by ray tracing, as discussed in the previous sections. The perturbations caused by the anomaly on the reflections coming from a deeper reflector (3.2 s on the nearest offset section), and for p_h equal to .04 km/s, are shown in Figure 23. Also in this case, the perturbations in transformed offsets caused by the anomaly are clear and consistent with my theory.

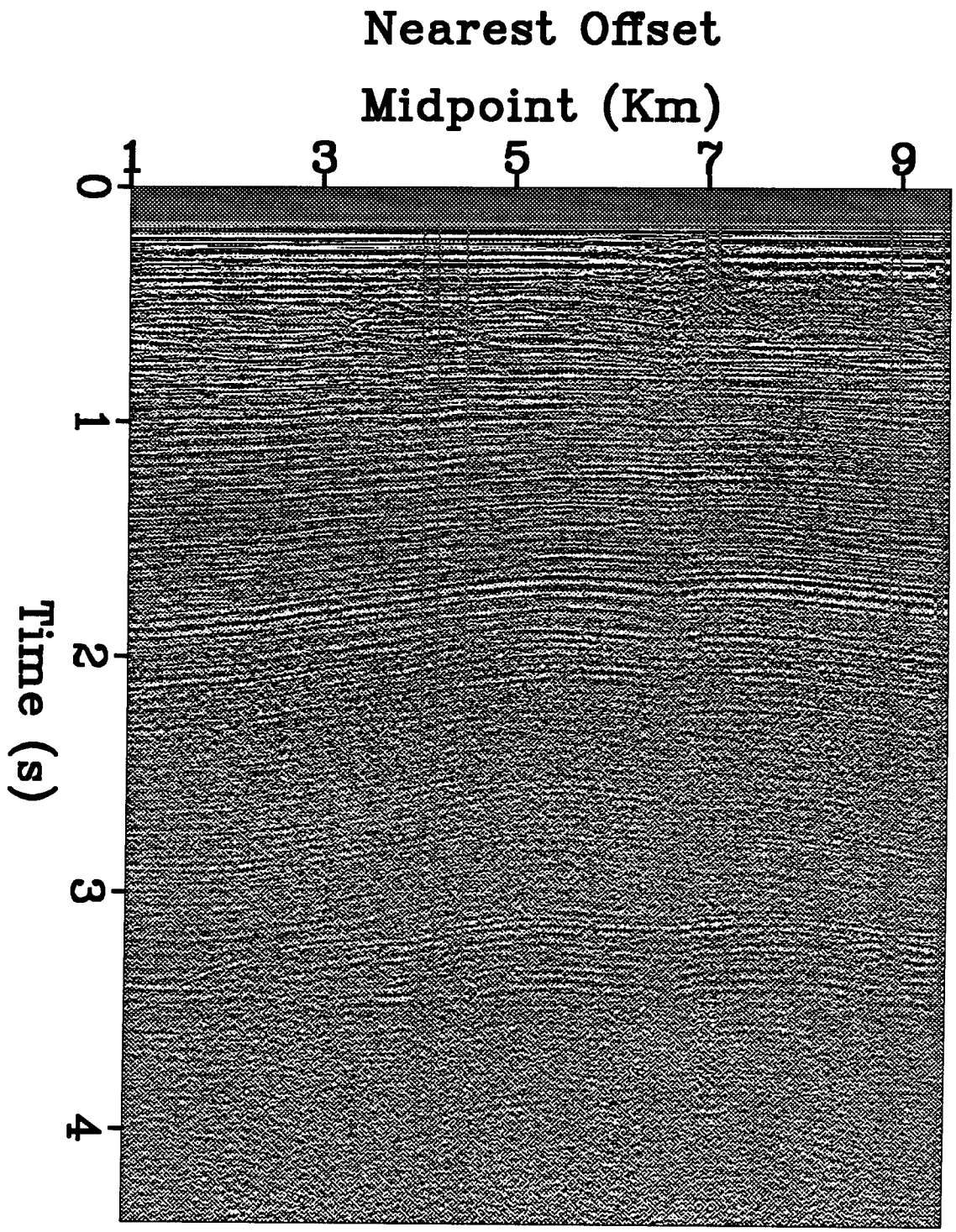

FIG. 19. The nearest-offset section of the marine data on which I will test the velocity estimation method. The data is interesting because of the low-velocity anomaly that causes the time pull-downs near the midpoint location of 7 km.

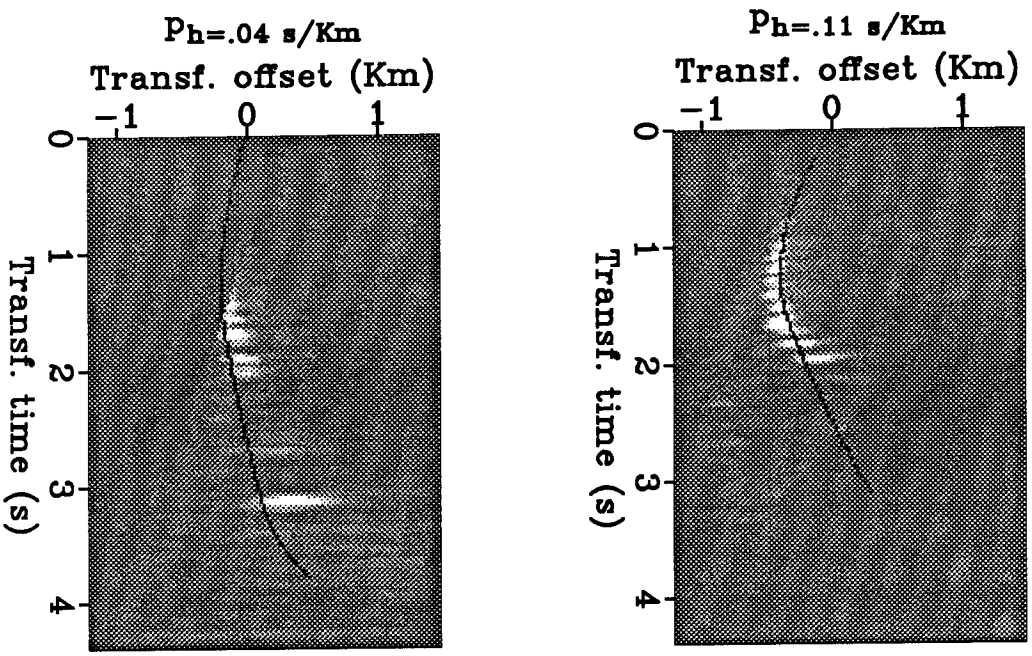

FIG. 20. Transformed beam stacks for two values of the offset ray parameter at the midpoint location of 6.650 km. This midpoint location is just above the anomaly and thus the transformed offsets are larger than the ones predicted by the laterally invariant background velocity (black lines).

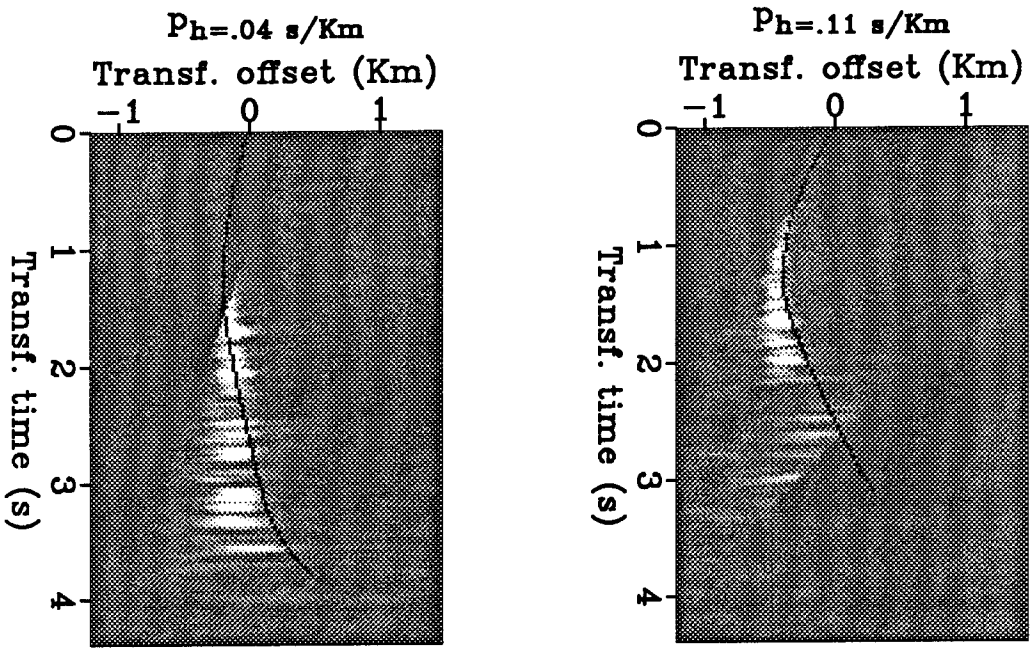

FIG. 21. Transformed beam stacks for two values of the offset ray parameter at the midpoint location of 7.650 km. This midpoint location is on the right of the anomaly and thus the transformed offsets are lower than the ones predicted by the laterally invariant background velocity (black lines).

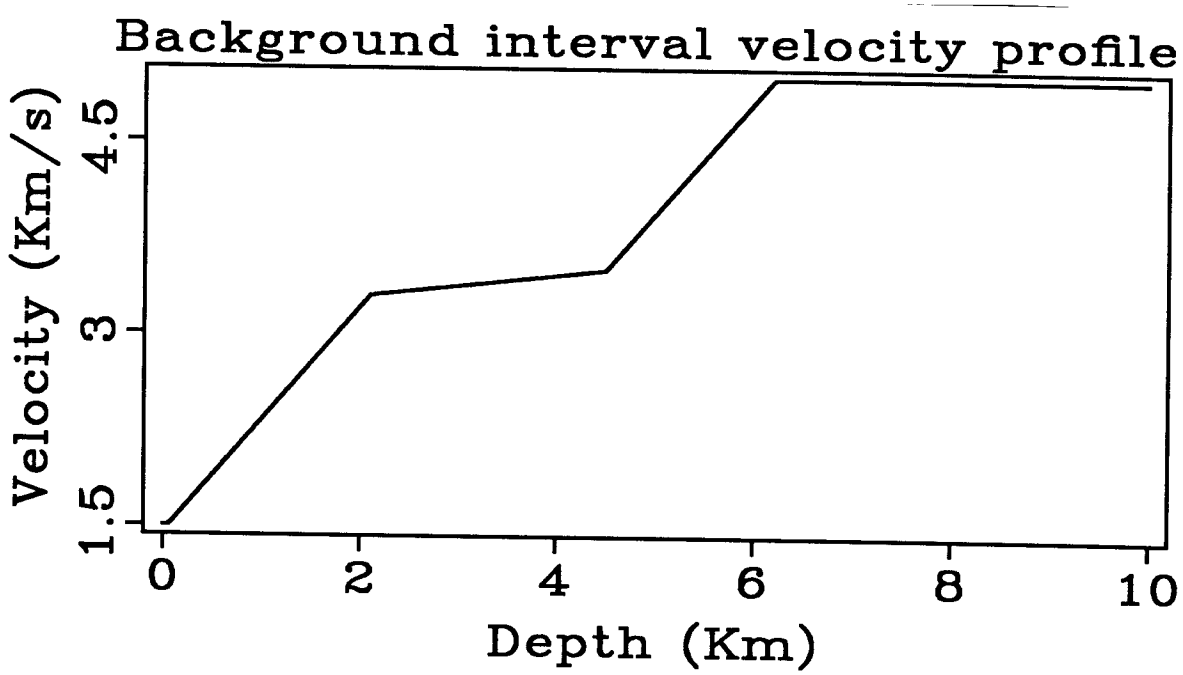

FIG. 22. The laterally invariant background velocity used to predict the transformed offsets curves superimposed on the beam stacks in the two previous figures.

CONCLUSIONS

A velocity anomaly causes perturbations in beam-stack offsets and traveltimes. These perturbations measured from the beam-stacks of a synthetic data set, modeled using finite-difference, are well predicted by ray tracing. Therefore ray tracing can be efficiently used in a velocity estimation procedure for predicting the offsets and traveltimes of beam-stacks and their gradient with respect to velocity.

The velocity anomaly causes different perturbations for different offset ray parameters of the reflections. The information contained in beam-stacked data with multiple offset ray parameters can be used for improving the resolution of the estimation, given the limitations in angular coverage of the anomaly imposed by the reflectors' geometry.

The preliminary analysis of a real data set containing a low-velocity anomaly shows that the predicted perturbations in beam-stacked data can be clearly measured from real data.

ACKNOWLEDGMENTS

I would like to thank Agip - Hydrocarbon Exploration and Deutsche Shell for making available the real data I used.

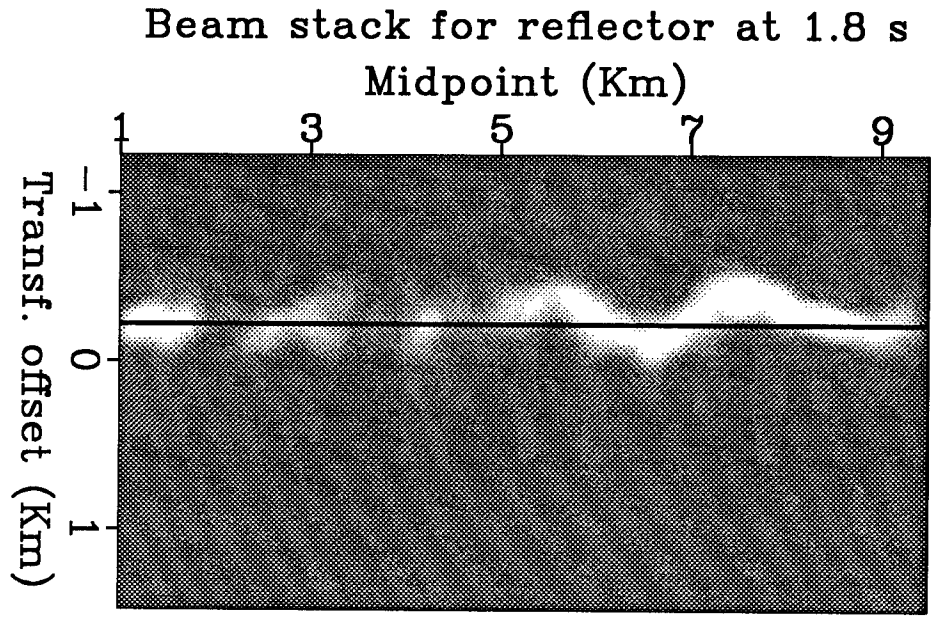

FIG. 23. Semblance as a function of transformed offset and midpoint location, for the reflection at about 1.8 s in the nearest-offset section. The perturbation pattern caused by the anomaly is similar to the perturbation pattern predicted by ray tracing.

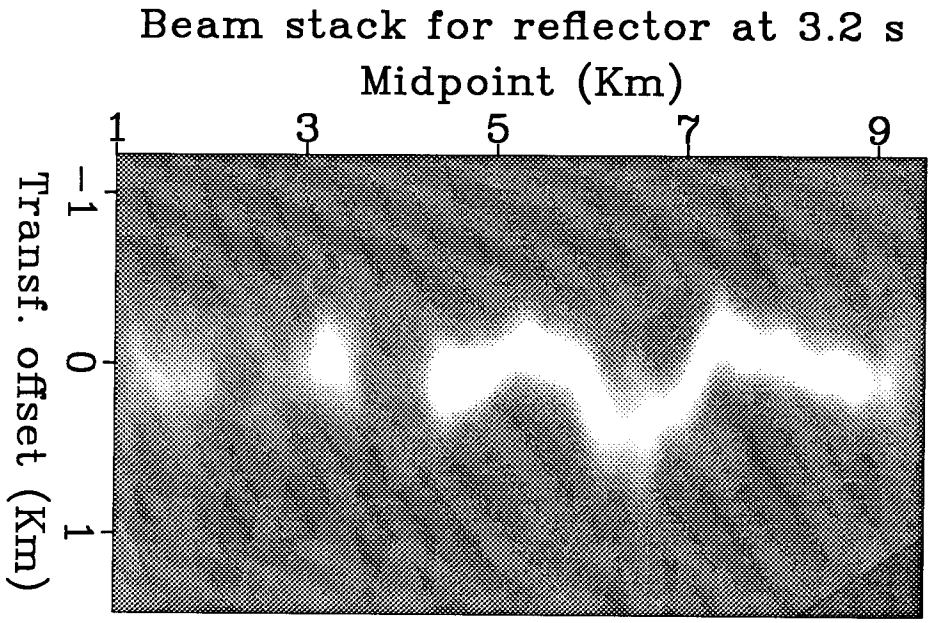

FIG. 24. Semblance as a function of transformed offset and midpoint location, for the reflection at about 3.2 s in the nearest-offset section. The perturbation pattern caused by the anomaly is similar to the perturbation pattern predicted by ray tracing.

The synthetic data set was generated by an acoustic modeling program written by John Etgen. As so often in the past, I greatly benefited from discussions on the velocity estimation problem with my office-mates Jos Van Trier and John Etgen.

REFERENCES

Biondi, B., 1987, Interval velocity estimation from beam-stacked data: SEP–**51**, 13–27.

Biondi, B., 1988, Interval velocity estimation from beam-stacked data — an improved method: SEP–**57**, 99–115.

Biondi, B., 1988, Interval velocity estimation from beam-stacked data — 2-D gradient operator: SEP–**59**, 103–120.

Bishop, T.N., Bube, K.P., Cutler, R.T., Langan, R.T., Love, P.L., Resnick, J.R., Shuey, R.T., Spindler, D.A., and Wyld, H.W., 1985, Tomographic determination of velocity and depth in laterally varying media: Geophysics, **50**, 903–923.

Fowler, P., 1988, Seismic velocity estimation using prestack time migration: Ph.D. thesis, Stanford University.

Gill, P.E., Murray, W., and Wright, M.H., 1981, Practical optimization: Academic Press Inc.

Harlan, B., and Burridge, R., 1983, A tomographic velocity inversion of unstacked data: SEP-**37**, 1-7.

Hermont, A.J., 1983, Letter to the editor, re: Seismic controllable directional reception as practiced in the U.S.S.R.: Geophysics, **44**, 1601–1602.

Kostov, C., and Biondi, B., 1987, Improved resolution of slant stacks using beam stacks: SEP–**51.**, 343–350.

Stork, C., 1988, Travel time tomography velocity analysis of seismic reflection data: Ph.D. thesis, Caltech.

Sword, C.H., 1987, Tomographic determination of interval velocities from reflection seismic data: The method of controlled directional reception: Ph.D. thesis, Stanford University.

Toldi, J.L., 1985, Velocity analysis without picking: Ph.D. thesis, Stanford University.

APPENDIX A

In this appendix I derive p_{heq} as a function of p_h, $\hat{p}_y$ and $\hat{V}$, for applying the transformation of coordinates introduced in equation (1b). The purpose of the transformation is to concentrate the beam-stacked data around the value $\xi = 0$; consequently for the reflections with ray parameters p_h and $\hat{p}_y$ it must be

$$p_{heq}(p_h, \hat{p}_y, \hat{V}) = \frac{4h}{\hat{V}^2 t}. \qquad (A1)$$

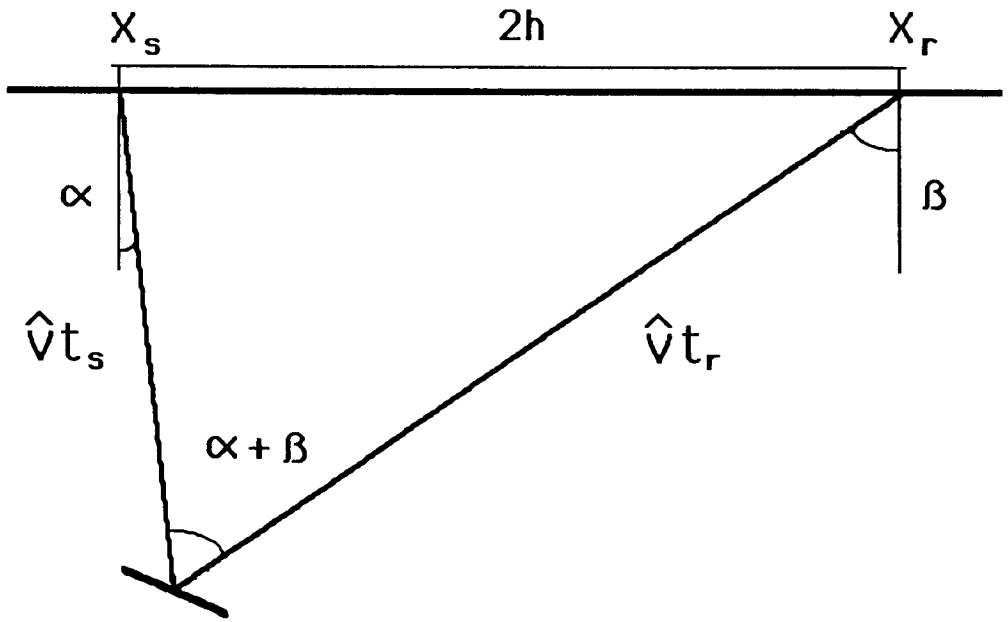

FIG. 25. The geometry of a reflection when the velocity is constant and equal to $\hat{V}$.

When $\hat{p}_y$ is equal to zero p_{heq} is simply equal to p_h (Biondi, 1988a), but its expression is more complicated if $\hat{p}_y$ is different from zero. Figure 25 shows the geometry of a reflection when the velocity is constant and equal to $\hat{V}$. The following identities can be derived from elementary trigonometric relations,

$$\frac{2h}{\sin(\alpha+\beta)} = \frac{\hat{V}t_s}{\cos\beta} = \frac{\hat{V}t_r}{\cos\alpha}; \tag{A2}$$

and with little algebraic manipulation I derive

$$h = \frac{\hat{V}\sin(\alpha+\beta)}{2(\cos\alpha+\cos\beta)}(t_s+t_r) = \frac{\hat{V}\sin(\alpha+\beta)}{2(\cos\alpha+\cos\beta)}t. \tag{A3}$$

Substituting h given by the previous expression in equation (A1) it follows that the value of p_{heq} that must be used in equation (1b) is

$$p_{heq} = \frac{2\sin(\alpha+\beta)}{\hat{V}(\cos\alpha+\cos\beta)}; \tag{A4}$$

where the angles α and β are related to the ray parameters by the following identities

$$\alpha = \arcsin(-\hat{V}p_s) = \arcsin\left[\frac{\hat{V}(p_h-p_y)}{2}\right], \tag{A5a}$$

and

$$\beta = \arcsin(\hat{V}\, p_r) = \arcsin\left[\frac{\hat{V}\,(p_h + p_y)}{2}\right]. \qquad (A5b)$$